

Chapter 11

Dielectrophoretic Characterization and Continuous Separation of Cells in a PDMS Microfluidic Device with Sidewall Conducting PDMS Composite Electrodes

Nuttawut Lewpiriyawong and Chun Yang

Abstract A complete polymer microfluidic device with sidewall conducting PDMS composite electrodes represents a new class of dielectrophoresis (DEP) devices used for manipulation of cells. This chapter summarizes the key functions of such a novel device for characterization of cells in stagnant flow and for continuous-flow separation of microparticles and cells based on size or electrical polarizability. These novel conducting PDMS composites can be synthesized by mixing 1 μm silver particles into PDMS gel. Unlike other existing fabrication techniques relying heavily on glass and silicon, the proposed technique yields sidewall conducting PDMS electrodes which are strongly bonded to PDMS microfluidic channels and allows for straightforward device assembly with only one-step oxygen plasma treatment.

11.1 Introduction

Separation of target cells in biofluids such as blood or bone marrow is one of the most important bioanalytical tasks for medical practitioners to diagnose patients' pathological states [1]. These complex biofluids usually contain various biosamples such as healthy cells, cancer cells, and even pathogenic microorganisms (e.g., *E. coli* O157:H7). Some of them are of similar sizes but possess different electrical properties; some are of similar electrical properties but have different sizes. For example, MCF10A, MDA-MB-231, and MCF7 human breast cancer cells are of similar sizes but not much difference in electrical properties [2]. Normal erythrocytes become less electrically conductive as they are injected by malaria

N. Lewpiriyawong • C. Yang (✉)
School of Mechanical and Aerospace Engineering, Nanyang Technological University,
50 Nanyang Avenue, Singapore 639798, Singapore
e-mail: lewp0001@e.ntu.edu.sg; mcyang@ntu.edu.sg

(*Plasmodium falciparum*) [3]. On the other hand, lymphocytes, monocytes, and granulocytes are white blood cells having similar electrical properties but are different in size [4].

Dielectrophoresis field-flow fractionation (DEP-FFF) has been proposed for separating cells in continuous flow [5]. DEP-FFF transports cells with pressure-driven flow in microfluidic channels and separates them using an externally applied DEP force perpendicular to the direction of flow. Under a nonuniform electric field, polarizable cells in a buffer solution can be manipulated by the DEP force as a result of polarization effects [6]. Since the magnitude and the direction of the DEP force is dependent on the polarizability of cell relative to that of buffer solution and its magnitude is also scaled to the cubic power of the cell radius, cells can be separated based on their size or polarizability without any pretreatment [7]. These intriguing benefits enable DEP to be a label-free, inexpensive and versatile separation tool, superior to flow cytometry where modification of samples with expensive reagents is often required [8].

To produce a DEP force, the conventional approach of generating a nonuniform electric field in DEP devices is through planar metallic electrodes deposited on the bottom or/and the top of the separation channel [9–11]. However, the rapid decay of electric field strength from the electrode surface often causes inefficient manipulation of cells at the center of the separation channel [12, 13]. As a result, three dimensional (3-D) or sidewall electrodes have been engineered to generate a 3-D electric field across the channel height. Recently reported 3-D electrodes are made from heavily doped silicon [14], pyrolytic SU-8 photoresist [15], electroplated gold or titanium [16, 17]. Nevertheless, the assembly of these devices is still rather complicated to prevent liquid leakage as the devices are fabricated from glass or silicon.

With the rapid advancement of soft lithography techniques, the use of polydimethylsiloxane (PDMS) as the fabrication material is ubiquitous in microfluidic devices due to its numerous advantages (e.g., ease of fabrication and bonding, low cost, biocompatibility, and optical transparency) [18]. However, a serious challenge is the infeasibility to embed 3-D metallic electrodes in PDMS-based DEP devices, since the adhesion between metallic electrodes and PDMS is extremely weak [19]. Manually embedding copper electrodes into PDMS channel to a certain degree overcomes the problem [20, 21], but this technique is not practical for batch fabrication and also readily causes liquid leakage at high flow rates due to the mismatch between the thickness of copper sheet and that of channel height.

Here we introduce a complete polymer DEP device with sidewall conducting PDMS composite electrodes for manipulating particles and biological cells [22, 23]. The proposed fabrication technique allows for very strong adhesion between the conducting PDMS composite electrodes and PDMS microfluidic channels, thus greatly facilitating the device assembly with only one-step oxygen plasma treatment. This novel device with sidewall conducting PDMS composite electrodes is so versatile that it can be employed for characterizing cells in stagnant flow and separating particles or cells based on their size or their polarizability.

11.2 Basic Theory of Dielectrophoresis

DEP is referred to as the motion of a neutrally charged particle suspended in a dielectric medium under a nonuniform electric field, and physically it results from the interaction between the induced dipoles in the polarized particle and the applied nonuniform electric field [7]. To provide a better understanding of how polarization occurs, two scenarios are described: a neutral particle is placed in both uniform and nonuniform electric fields. As shown in Fig. 11.1a, under an applied electric field, both particle and medium are polarized and dipole charges are induced in the particle. When the electric field is uniform, columbic forces acting on induced net dipole charges (on both sides) are equal in magnitude but opposite in direction. Therefore, the net force is zero and the particle has no movement. This phenomenon

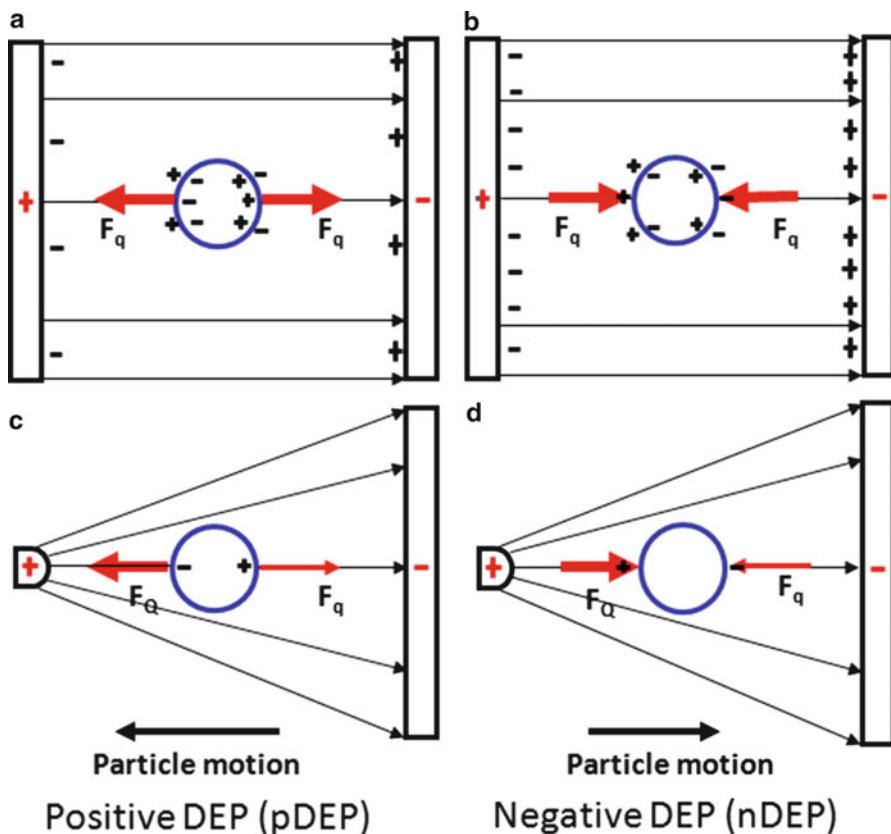


Fig. 11.1 Motion of a neutrally charged particle under an applied electric field [24]. A neutral particle (a) more or (b) less polarizable than the suspending medium has no movement under an applied uniform electric field due to zero net force. Under a nonuniform electric field the net force acting on the particle however is no longer zero. (c) When a particle is more polarizable than the suspending medium, the particle is attracted to the high electric field region as $F_Q > F_q$. (d) When a particle is less polarizable than the suspending medium, the particle is repelled from the high electric field region as $F_q > F_Q$

occurs for the particle either more or less polarizable than the suspending medium as shown in Fig. 11.1a, b, respectively. On the other hand, consider a particle more polarizable than the medium in a spatially nonuniform electric field (Fig. 11.1c). Because the electric field near the left electrode is higher, the columbic force on the left side is larger ($F_Q > F_q$). As a result, the net force attracts the particle to the high electric field region. This motion is known as positive DEP (pDEP). In contrast, when a particle is less polarizable than the suspending medium, the net force repels the particle to be away from the high electric field region (Fig. 11.1d). This motion is known as negative DEP (nDEP).

Under an AC electric field, $\vec{E}_{ac}(\vec{r}, t)$, the DEP force acting on a dielectric particle can be quantified by using the effective dipole moment method [25]. Assuming that the particle and suspending medium have dielectric permittivities of ϵ_p and ϵ_m , and conductivities of σ_p and σ_m , respectively, the time-average DEP force acting on the particle with radius a can be expressed as

$$\langle \vec{F}_{DEP} \rangle = 2\pi\epsilon_m a^3 \overline{Re[K^*(\omega)]} \nabla E_{rms}^2 \quad (11.1)$$

where $\langle \rangle$ denotes the time-average, $E_{rms,ac} = \vec{E}_{ac}/\sqrt{2}$ is the root-mean-square magnitude of the applied AC electric field and ∇ denotes a gradient operator. $Re[K^*(\omega)]$ is the real part of the Clausius-Mossotti (CM) factor and $-0.5 \leq Re[K^*(\omega)] \leq 1$. $K^*(\omega)$ is a function of electric field frequency and complex permittivities of the particle and the suspending medium, and it can be expressed as

$$K^*(\omega) = \frac{\epsilon_p^* - \epsilon_m^*}{\epsilon_p^* + 2\epsilon_m^*} \quad (11.2)$$

where $\epsilon_p^* = \epsilon_p - i\sigma_p/\omega$ and $\epsilon_m^* = \epsilon_m - i\sigma_m/\omega$ are the complex permittivities of the particle and the suspending medium, respectively, $i = \sqrt{-1}$, and $\omega = 2\pi f$ is the radian field frequency. From (11.1), under the same applied electric field condition, the sign and magnitude of the DEP force depends on both $Re[K^*(\omega)]$ and particle size. When $Re[K^*(\omega)] > 0$, it is indicated that the particle is more polarizable than the suspending medium and it experiences a pDEP force (Fig. 11.1c). On the other hand, $Re[K^*(\omega)] < 0$ indicates that the particle is less polarizable than the suspending medium and it experiences an nDEP force (Fig. 11.1d). Furthermore, as $Re[K^*(\omega)]$ becomes zero, both particle and the suspending medium are equally polarizable and the corresponding frequency is known as the cross-over frequency where the DEP force vanishes. Therefore, cells of the same size possessing distinct polarizabilities (nDEP and pDEP) can be separated from each other. In some cases where cells have the same polarizability but are of different size, larger cells experiencing a stronger nDEP force can be repelled farther away from the high electric field region than the smaller ones, thus achieving separation. In addition, due to the complex structure of biological cells such as yeast and bacterial cells, the CM factor can be determined by modeling the structure of a cell as consisting of three concentric layers. For yeast cells, the three layers are wall, cytoplasm, and nucleus [26]. For bacterial cells, the

three layers are wall, membrane, and cytoplasm [27]. The CM factor is then given by

$$K^*(\omega) = \frac{\epsilon_{\text{cell}}^* - \epsilon_{\text{m}}^*}{\epsilon_{\text{cell}}^* + 2\epsilon_{\text{m}}^*} \quad (11.3)$$

where ϵ_{cell}^* is the effective complex permittivity of the cell. Using the smeared-out sphere approach [28], one can obtain the effective complex permittivity of the cell as

$$\epsilon_{\text{cell}}^* = \epsilon_1^* \left[\frac{\left(\frac{r_1}{r_2}\right)^3 + 2\left(\frac{\epsilon_{23}^* - \epsilon_1^*}{\epsilon_{23}^* + 2\epsilon_1^*}\right)}{\left(\frac{r_1}{r_2}\right)^3 - \left(\frac{\epsilon_{23}^* - \epsilon_1^*}{\epsilon_{23}^* + 2\epsilon_1^*}\right)} \right] \quad (11.4)$$

and

$$\epsilon_{23}^* = \epsilon_2^* \left[\frac{\left(\frac{r_2}{r_3}\right)^3 + 2\left(\frac{\epsilon_3^* - \epsilon_2^*}{\epsilon_3^* + 2\epsilon_2^*}\right)}{\left(\frac{r_2}{r_3}\right)^3 - \left(\frac{\epsilon_3^* - \epsilon_2^*}{\epsilon_3^* + 2\epsilon_2^*}\right)} \right] \quad (11.5)$$

where ϵ_1^* , ϵ_2^* , ϵ_3^* , r_1 , r_2 , and r_3 are the complex permittivities and radii of (1) yeast cells' wall, cytoplasm, and nucleus or (2) bacterial cells' wall, membrane, and cytoplasm, respectively.

11.3 PDMS Microfluidic Device with Sidewall Conducting PDMS Composite Electrodes

Conducting PDMS composites were synthesized by adding 1 μm silver (Ag) particles into PDMS gel and using them as sidewall DEP electrodes in a PDMS-based micro flow device, as shown in Fig. 11.2a. The device fabrication processes were elaborated in detail in our previous work [22]. The device has a 200 μm wide and 1,400 μm long separation channel with four branch channels connected to inlets A and B and outlets C and D. The branch channels A, B, C, and D are 100, 115, 50, and 170 μm wide, respectively. The depth of all channels is 40 μm . Four 100 μm wide AgPDMS electrodes with 100 μm separating gaps apart were embedded along a sidewall of the separation channel.

The following key functions of such a device have been demonstrated: (1) DEP characterization of cells in stagnant flow, (2) continuous-flow separation of cells from latex particles by polarizability, and (3) continuous-flow separation of microparticles by size. The DEP characterization of yeast and bacterial cells was

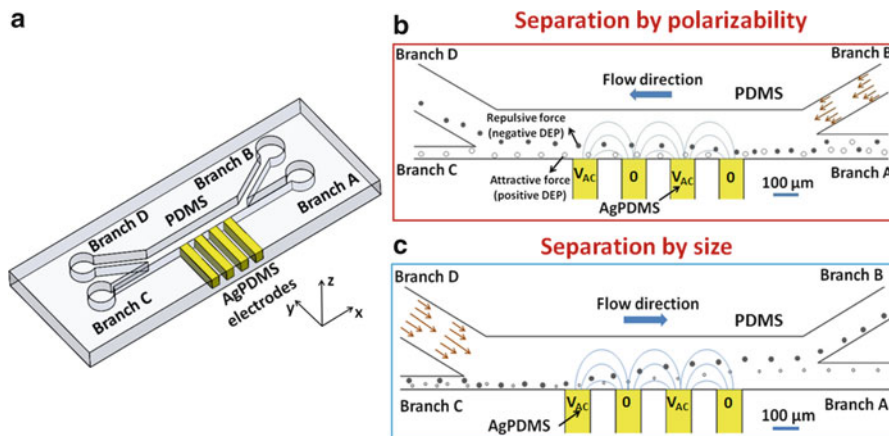


Fig. 11.2 (a) Schematic of a PDMS-fabricated microfluidic device with sidewall conducting AgPDMS composite electrodes. (b) Schematic of continuous separation of samples of similar sizes by polarizability [23]. In this operation mode, the device separates the samples under pDEP to the lower branch C and the others under nDEP to the upper branch D. (c) Schematic of continuous separation of samples of two different sizes but having the same polarizability [22]. The device separates larger samples (undergoing a larger nDEP force) to the upper branch B and smaller samples to the lower branch A ((a) and (c) are adapted with permission from Lewpiriyawong et al. (2010). ©2010 WILEY-VCH Verlag GmbH & Co. KGaA; (b) is reprinted with permission from Lewpiriyawong et al. (2011). ©2011 American Chemical Society)

performed in stagnant buffer solutions under a broad spectrum of AC electric field frequencies (i.e., 10 kHz to 80 MHz). Accommodating this parameter allows for an investigation of frequency-dependent DEP behaviors of cells, which are useful information for separating different kinds of cells. In addition to the characterization, this device can be operated to separate particles and cells, depending on either their polarizability or size.

11.3.1 Separation of Samples by Polarizability

Figure 11.2b illustrates the separation of cells from particles of similar sizes by pDEP and nDEP forces, respectively, due to their different polarizabilities. In particular, the samples containing a mixture of cells and particles from branch A are first hydrodynamically focused by the flow from branch B such that the focused samples can experience a strong DEP force near the electrodes. Then, the cells undergoing pDEP are attracted to the electrodes and are transported to the lower branch C, while the particles undergoing nDEP are repelled away from the electrodes being transported to the upper branch D.

11.3.2 Separation of Samples by Size

Figure 11.2c illustrates the separation of particles having the same polarizability (i.e., nDEP) by size. As larger particles experience a stronger repulsive nDEP force, they are pushed laterally farther away from the electrodes in comparison to the smaller particles. When the applied voltage is large enough, the larger particles can be transported to the upper branch B separating them from the smaller ones, which are transported to the lower branch A.

11.4 Results and Discussion

11.4.1 Numerical Simulation of Electric Fields and DEP Forces

In a microchannel with sidewall AgPDMS composite electrodes, the electric field $\vec{E} = -\nabla\phi$ associated with the electric potential ϕ is governed by Laplace's equation ($\nabla^2\phi = 0$). The boundary conditions are specified based on the channel configuration shown in Fig. 11.2a. The component of the electric field normal to the nonconducting PDMS walls as well as all inlets and outlets are set to be zero, the first and third electrodes (from the left) are assigned with an electric potential ($\phi = V_{AC}$), and the potentials of the second and fourth electrodes are also set to be zero ($\phi = 0$). The contour electric fields (lines) and DEP forces (arrows) created by the sidewall AgPDMS electrodes are numerically obtained using COMSOL Multiphysics (version 3.4). As shown in Fig. 11.3a, when $Re[K^*(\omega)] < 0$, nDEP forces cause the repulsion of cells away from the sidewall electrodes. The opposite scenario (cell attraction to the electrodes) occurs when $Re[K^*(\omega)] > 0$, as shown in Fig. 11.3b. The magnitude of the DEP forces shown by arrows are proportional to the length of arrows. The simulation results also indicate that highly nonuniform electric fields are induced near the AgPDMS electrode edges as can be seen from the high density of accumulated electric field lines. However, electric field strength rapidly decreases at further distance from the electrodes (along the y direction). Such an electric field distribution results in markedly strong DEP forces near the electrodes. Furthermore, along the horizontal direction, the DEP force is much weaker towards both the center of the electrode and the center of the gap between any two adjacent electrodes. Therefore, for all samples of experiencing dominant DEP force effects, the hydrodynamic focusing is incorporated in our two separation mechanisms to confine the flowing particle stream near the edges of the sidewall electrodes.

11.4.2 DEP Characterization of Yeast and Bacterial Cells

DEP behaviors of yeast and bacterial cells were characterized under various AC electric field frequencies ranging from 10 kHz to 80 MHz in stagnant buffer

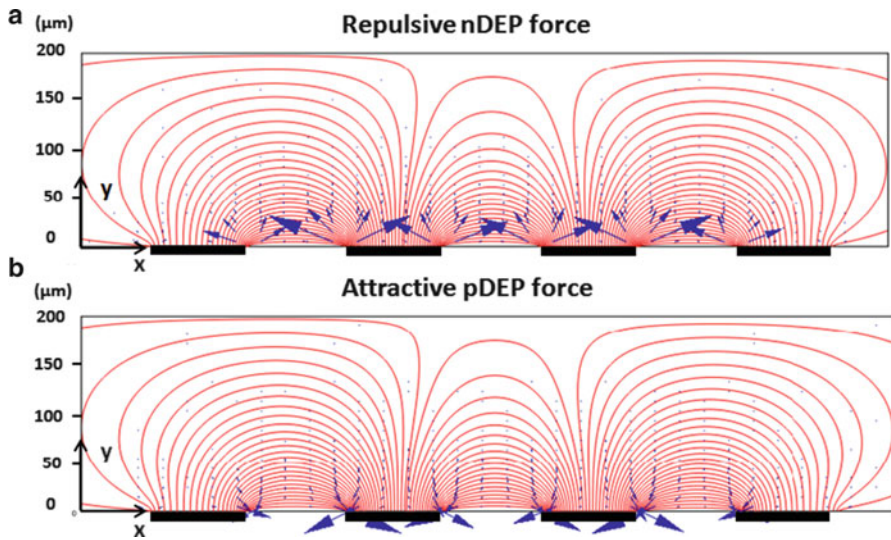


Fig. 11.3 Numerical simulation of the contour electric fields (*lines*) and DEP forces (*arrows*) created by sidewall AgPDMS electrodes (*thick black segments*). (a) nDEP forces cause repulsion of cells away from the electrodes, while (b) pDEP forces point towards the electrodes resulting in attraction of cells. These DEP forces are shown by *arrows* with their length proportional to the magnitude of force

solutions. The effects of medium conductivity on cellular DEP behavior were investigated by suspending the cells in $2 \mu\text{S}/\text{cm}$ DI water and $380 \mu\text{S}/\text{cm}$ NaCl solution. Based on (11.3) together with (11.4) and (11.5), the real part of the CM factor predicts the frequency-dependent DEP responses of yeast and bacterial cells whether they both experience either pDEP or nDEP, depending on the specific frequency and buffer solution as shown in Fig. 11.4a. These predicted behaviors were computed by basing them on the cell's structural dimensions and dielectric properties taken from the literature [27, 29]; they were verified experimentally through the use of conducting PDMS composite electrodes.

Figure 11.4b presents well dispersed yeast cells in stagnant $380 \mu\text{S}/\text{cm}$ NaCl solution under no applied electric field. With an AC voltage of 10 V at 10 kHz, yeast cells underwent a repulsive nDEP force and were moved away from the electrodes (Fig. 11.4c). This behavior is consistent with the CM factor prediction which explains that yeast cells are less polarizable than the $380 \mu\text{S}/\text{cm}$ NaCl solution at 10 kHz. More findings from the literature [30–32] confirmed that yeast cells tend to exhibit nDEP in the low frequency regime. On the other hand, at 10 MHz, yeast cells underwent an attractive pDEP force, thus being transported towards and accumulating at the electrodes' edges (Fig. 11.4d). Above 80 MHz, no DEP movement of cells could be noticed. This was anticipated, since at very high frequencies the computed effective complex permittivity of yeast cells is rather close to the permittivity of the buffer solution, the resulting CM factor becomes small at 80 MHz (Fig. 11.4a). Hence, the DEP force became insignificant in the experiments. Moreover, the device can

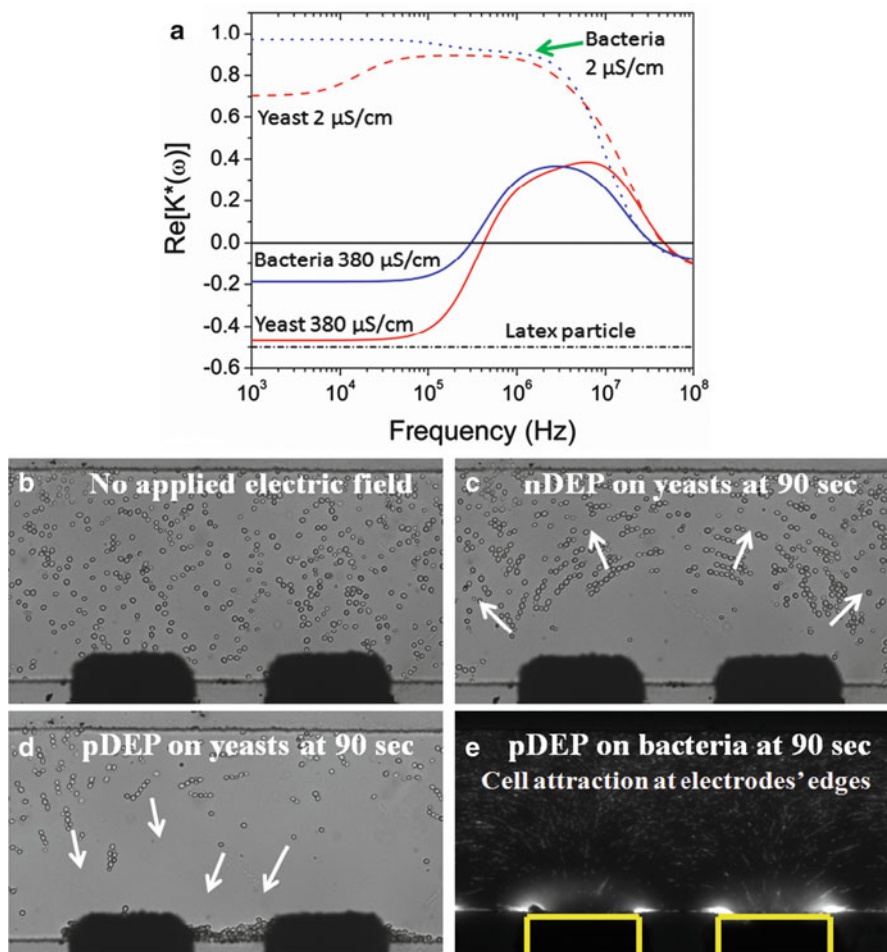


Fig. 11.4 (a) CM factor versus electric field frequency for yeast and bacterial cells in $2 \mu\text{S/cm}$ DI water and $380 \mu\text{S/cm}$ NaCl solution and for latex particles in $380 \mu\text{S/cm}$ NaCl solution. The structural dimensions and dielectric properties of these cells are taken from the literature [27, 29]. (b–e) DEP behaviors of yeast and bacterial cells in stagnant NaCl solution of $380 \mu\text{S/cm}$. (b) Well dispersed yeast cell suspension in the absence of applied AC electric field. (c) Cells experience a repulsive nDEP force after 90 s under 10 V at 10 kHz [23]. (Reprinted with permission from Lewpiriyawong et al. (2011). ©2011 American Chemical Society). (d) Cells experience an attractive pDEP force after 90 s under 10 V at 10 MHz. (e) Accumulation of *E. coli* after 90 s by an attractive pDEP force under 15.3 V at 1 MHz. These snapshot images were captured with a $20\times$ objective

reasonably provide the cross-over frequencies as compared to the predicted ones. The DEP behaviour of yeast cells was found to change from nDEP to pDEP at ~ 300 kHz and from pDEP to no DEP at ~ 40 MHz. At these applied AC field frequencies, cells could not move due to the DEP force being zero.

Additional experimental findings showed that reducing the medium conductivity from 380 to 2 $\mu\text{S}/\text{cm}$ can result in a change from nDEP to pDEP at low frequencies. According to (11.3), such switching of DEP behavior is expected when the medium conductivity is lower than that of the cell (i.e., $\sigma_m < \sigma_{\text{cell}}$). Experiments using conducting AgPDMS electrodes clearly confirmed this DEP switching. For all frequencies ranging from 10 kHz up to a cross-over frequency of 40 MHz, yeast cells suspended in 2 $\mu\text{S}/\text{cm}$ DI water were observed to experience only a pDEP force, attracting them to the electrodes (images are not shown here but the cell behavior under pDEP are similar to that shown in Fig. 11.4d). Above the cross-over frequency of 40 MHz, cells no longer moved under the applied AC field because the DEP force became very weak (as shown by the red dashed line at 40 MHz shown in Fig. 11.4a). In addition, cells were also observed to form chains in the same direction as the electric field lines as shown in Fig. 11.3. The mechanism of chain formations has been described in the literature [25]. It is also important to note that in DI water, Baker's yeast cells still survive though experiencing a high osmotic pressure[33].

DEP behavior of *E. coli* cells was also obtained through the use of conducting AgPDMS electrodes. Under an AC voltage of 15.3 V at 400 kHz and 30 MHz, *E. coli* cells in 380 $\mu\text{S}/\text{cm}$ NaCl solution exhibited weak pDEP but strong pDEP at 1 MHz (Fig. 11.4e). These DEP behaviour regimes are reasonably consistent with the CM factor prediction in Fig. 11.4a, although no DEP movement was experimentally observed below 150 kHz and above 35 MHz. Moreover, two cross-over frequencies were found at 150 kHz (from no DEP to pDEP) and 35 MHz (from pDEP to no DEP). Similar in behavior to the yeast cells, *E. coli* cells suspended in DI water only experienced pDEP at all frequencies from 10 kHz to 30 MHz, even up to a cross-over frequency of 35 MHz. Formation of an *E. coli* chain was noted in that cells aligned along the electric field lines.

In general, the DEP behavior and the cross-over frequencies of yeast and bacterial cells are quite similar. They experienced nDEP in the low frequency regime (e.g., 10–100 kHz) and pDEP in the medium-to-high frequency regime (e.g., 500 kHz to 10 MHz). On one hand, at low frequencies, the CM factor is mainly determined by the conductivity of the cell and the buffer solution. Since their membrane conductivity is very low, biological cells behave like insulating objects under a DC or low frequency electric field, thus experiencing nDEP [30]. On the other hand, at higher frequencies, an electric current can pass through the capacitive membrane and the conductivity of the cells is dominated by the relatively high conductivity of the internal parts of the cells. As a result, the cells tend to exhibit pDEP in the medium-to-high frequency regime. Furthermore, our experiments showed that *E. coli* cells are generally more conductive than yeast cells. This finding is validated from the experimental facts that in the 380 $\mu\text{S}/\text{cm}$ NaCl solution, *E. coli* cells experienced pDEP while yeast cells experienced nDEP at 10 kHz.

11.4.3 Continuous Separation of Samples by Polarizability

The separation of samples of similar sizes based on their different polarizabilities is demonstrated by subjecting one type of samples by nDEP and the others by pDEP. This separation mechanism, previously described in Sect. 11.3, is also shown in Fig. 11.2b. Three binary mixtures were prepared: (1) yeast cells and 5 μm fluorescent latex particles, (2) bacterial cells and 3 μm latex particles, and (3) live and dead yeast cells. These latex microspheres (of similar sizes to yeast and bacterial cells) were selected to eliminate the size-dependent effect.

As shown in Fig. 11.4a, the CM factor predicts that yeast cells and latex particles will exhibit distinct DEP polarizabilities at the medium range of the AC electric field frequency (i.e., from 300 kHz to 1 MHz) in 380 $\mu\text{S}/\text{cm}$ NaCl solution. The latex particles are predicted to experience nDEP for all frequencies since they are electrically insulating, and the resulting CM factor of latex particles approaches -0.5 . Figure 11.5a presents a snapshot image of the continuous-flow separation of yeast cells (black dots) by pDEP and 5 μm fluorescent latex particles (white dots) by nDEP under 31.2 V at 300 kHz (cross-over frequency of yeast cells) after 4 min. Both yeast cells and particles were hydrodynamically focused near the sidewall AgPDMS composite electrodes so as to have a strong DEP force as shown by the distribution of the simulated DEP force (Fig. 11.3). The latex particles were repulsed from the electrodes by the nDEP force and separated to outlet D. In contrast, as the yeast cells underwent a weak pDEP force, most of them ended up preferentially in outlet C, though the others were observed to be attracted to the electrodes. The rationale that yeast cells exhibited the weak pDEP force rather than zero DEP force at 300 kHz results from their DEP polarizability which is highly sensitive to frequency in this frequency regime. In these experiments, the time window defined by the velocity of the fluid flow (306 $\mu\text{m}/\text{s}$) and the separation channel length (1,400 μm) was about 4.6 s, giving rise to an nDEP drift velocity of about 11 $\mu\text{m}/\text{s}$. The separation of yeast cells (with a throughput $\sim 780/\text{min}$) and 5 μm latex particles (with a throughput $\sim 1,200/\text{min}$) were reliable for more than 5 min at the flow rate of 0.15 $\mu\text{l}/\text{min}$, and the separation efficiency was up to 97%.

Compared to yeast cells, separation of smaller samples like *E. coli* cells and 2.9 μm latex particles becomes more challenging as the DEP force—scaled to the cubic power of cell size—on these small cells is much weaker. Therefore, strong pDEP and nDEP forces are preferred for separating these two samples. Based on the CM factor shown in Fig. 11.4a, the most suitable AC electric field frequency to separate *E. coli* from the particles is 10 MHz, since it provides a strong pDEP force for *E. coli* and a strong nDEP force for the particles. However, the maximum frequency achievable by our customized amplifier is limited to 1 MHz to generate a higher voltage (40.4 Vac). Under 40.4 Vac at 1 MHz, clear separation of *E. coli* and 2.9 μm latex particles in 380 $\mu\text{S}/\text{cm}$ NaCl solution still can be successfully achieved as illustrated in Fig. 11.5b. This separation of *E. coli* (with a throughput $\sim 1,440/\text{min}$) and 2.9 μm latex particles (with a throughput $\sim 780/\text{min}$) were reliable at the flow rate of 0.06 $\mu\text{l}/\text{min}$ for more than 6.18 min with a separation efficiency

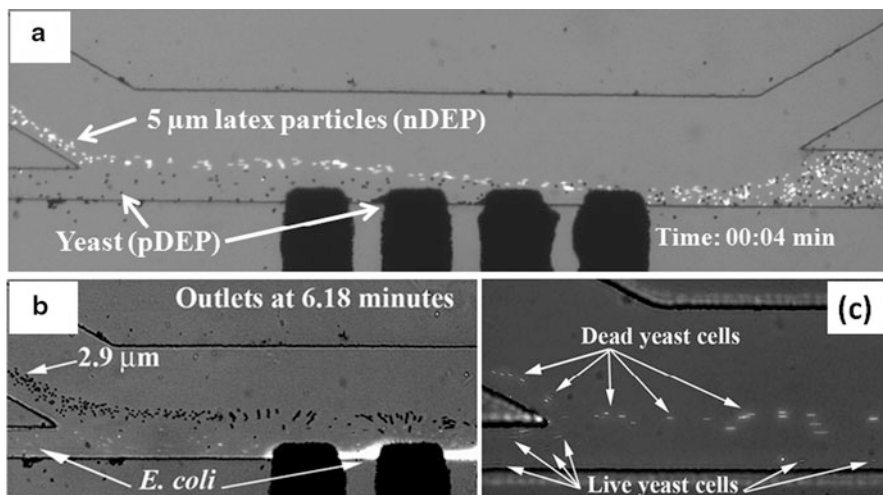


Fig. 11.5 Snapshot images of continuous separation of samples of similar sizes by polarizability [23]. (a) Separation of yeast cells (*black dots*) by pDEP from 5 μm fluorescent latex particles (*white dots*) experiencing nDEP under 31.2 Vac at 300 kHz after 4 min. (b) Separation of stained *E. coli* cells by pDEP from 2.9 μm latex particles exhibiting nDEP under 40.4 Vac at 1 MHz after 6.18 min. (c) Separation of live yeast cells by pDEP from dead yeast cells undergoing nDEP under 26.5 Vac at 1 MHz. The microscopic objective lenses used in (a), (b), and (c) are 5 \times , 10 \times , and 20 \times , respectively (Reprinted with permission from Lewpiriyawong et al. (2011). ©2011 American Chemical Society)

of up to 97%. In these experiments, the time window defined by the velocity of the fluid flow (123 $\mu\text{m}/\text{s}$) and the separation channel length (1,400 μm) was about 11.4 s, thus resulting in an nDEP drift velocity of about 4.4 $\mu\text{m}/\text{s}$.

In addition to the separation of biological cells from latex particles, the device was also tested to separate live and dead yeast cells based on the difference in their electrical properties. The demonstration was performed in a 600 $\mu\text{S}/\text{cm}$ NaCl solution. Huang et al. found that the conductivity of the nucleus of live yeast cells dramatically decreased from 0.2 to 7×10^{-3} S/m after they died [28]. The reason the nucleus's conductivity rapidly changes is because the membrane of dead yeast cells becomes more permeable and it permits content inside the cells to exchange with the external liquid medium [34]. Therefore, the dead cells are less conductive and hence are likely to experience nDEP in comparison with the live cells. Consistent with these experimental facts, our characterization results (images not shown here) revealed that at 1 MHz, live cells suspended in a 600 $\mu\text{S}/\text{cm}$ NaCl solution underwent pDEP while dead cells underwent nDEP. Figure 11.5c shows continuous-flow separation of live yeast cells (*black dots*) from dead ones (*white dots*) under 26.5 V at 1 MHz. Dead cells were repulsed from the electrodes by nDEP and transported to the upper outlet D, while live cells under pDEP were attracted to

the electrodes and ended up in the lower outlet C. The device was operated at a flow rate of $0.087 \mu\text{l}/\text{min}$ with a throughput of 480 cells/min for both samples. The separation efficiency was more than 97%. For these experiments, the time window defined by the velocity of the fluid flow ($181 \mu\text{m}/\text{s}$) and the separation channel length ($1,400 \mu\text{m}$) was about 7.7 s, thus leading to an nDEP drift velocity of about $6.5 \mu\text{m}/\text{s}$.

11.4.4 Continuous-Flow Separation of Samples by Size

As elaborated in Sect. 11.3 and illustrated in Fig. 11.2c, samples of different sizes but having the same polarizability (e.g., nDEP) can be separated by size. The DEP force expressed in (11.1) clearly shows that the magnitude of DEP force is proportional to the cubic power of particle radius. Thus, the larger particles attain a stronger nDEP force and can be diverted to the upper branch B, whereas the smaller ones, experiencing a weaker nDEP force, move to the lower branch A. Figure 11.6a shows continuous separation of $5 \mu\text{m}$ particles from $10 \mu\text{m}$ particles under 55 Vac at 1 MHz. The separation efficiency for $5 \mu\text{m}$ particles is 88% at the lower branch A and that for $10 \mu\text{m}$ particles is 100% at the upper branch B. Moreover, separation of 10 and $15 \mu\text{m}$ particles was also successfully achieved with a separation efficiency of 100% for both particle sizes as shown in Fig. 11.6b. Both separation experiments were operated at a flow rate of $0.68 \mu\text{l}/\text{min}$. By assessing the voltages required to achieve the separation of these two cases, the voltage for the second case (with larger particles) is anticipated to be lower than that for the first, since the larger particles attain a stronger DEP force under the same applied voltage.

11.5 Conclusions

This chapter presents manipulation of cells using DEP forces via sidewall PDMS composite electrodes in a complete polymer DEP device. Three main functions of the device are demonstrated, including (1) characterization of cell DEP behavior, (2) separations of cells from latex particles and live and dead cells by polarizability, and (3) separation of microparticles by size. The DEP characterization results reveal the excellent capability of conducting PDMS composite electrodes accurately to provide the desired DEP behavior regimes for both yeast and bacterial cells. Furthermore, the very high separation efficiency of $\sim 97\%$ for all cases (either by polarizability or by size) demonstrates that conducting PDMS composite electrodes have promising performance and versatility to deal with a variety of cells in biofluids.

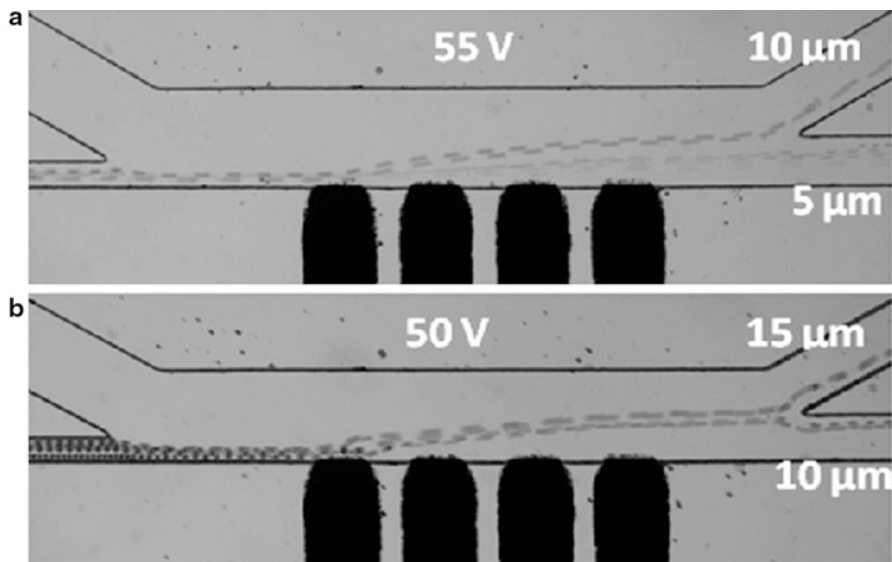


Fig. 11.6 Superimposed images of continuous separation of microparticles according to their size [22]. (a) Separation of 5 μm particles from 10 μm particles under 55 Vac at 1 MHz. (b) Separation of 10 μm particles from 15 μm particles under 50 Vac at 1 MHz. Both cases are operated at 0.68 μl/min. Separation of larger samples requires lower voltages since they experience a stronger DEP force (Reprinted with permission from Lewpiriyawong et al. (2010). ©2010 WILEY-VCH Verlag GmbH & Co. KGaA)

References

1. Toner M, Irimia D (2005) Blood on a chip. *Annu Rev Biomed Eng* 7:77–103
2. Henslee EA, Sano MB, Rojas AD, Schmelz EM, Davalos RV (2011) Selective concentration of human cancer cells using contactless dielectrophoresis. *Electrophoresis* 32:2523–2529
3. Gascoyne P, Mahidol C, Ruchirawat M, Satayavivad J, Watcharasitb P, Beckera FF (2002) Microsample preparation by dielectrophoresis: isolation of malaria. *Lab Chip* 2:70–75
4. Yang J, Huang Y, Wang X-B, Becker FF, Gascoyne PRC (2000) Differential analysis of human leukocytes by dielectrophoretic field-flow-fractionation. *Biophys J* 78:2680–2689
5. Schimpf ME, Caldwell K, Giddings JC (2000) Field-flow fractionation handbook. Principle and theory. Wiley, New York
6. Pohl HA (1951) The motion and participation of suspensoids in divergent electric fields. *J Appl Phys* 22(7):869–871
7. Pohl HA (1978) Dielectrophoresis—the behavior of neutral matter in nonuniform electric fields. Cambridge University Press, Cambridge
8. Lenshof A, Laurell T (2010) Continuous separation of cells and particles in microfluidic systems. *Chem Soc Rev* 39:1203–1217
9. Yang J, Huang Y, Wang X-B, Becker FF, Gascoyne PRC (1999) Cell separation on microfabricated electrodes using dielectrophoretic/gravitational field-flow fractionation. *Anal Chem* 71:911–918
10. Wang X-B, Yang J, Huang Y, Vykoukal J, Becker FF, Gascoyne PRC (2000) Cell separation by dielectrophoretic field-flow fractionation. *Acc Chem Res* 72:832–839
11. Moschalski M, Hausmann M, Posch A, Paulus A, Kunz N, Duong TT, Angres B, Fuchsberger K, Steuer H, Stoll D, Werner S, Hagemeyer B, Stelzle M (2010) MicroPrep: chip-based dielectrophoretic purification of mitochondria. *Electrophoresis* 31:2655–2663

12. Morgan H, Izquierdo AG, Bakewell D, Green NG, Ramos A (2001) The dielectrophoretic and travelling wave forces generated by interdigitated electrode arrays: analytical solution using Fourier series. *J Phys D Appl Phys* 34:1553–1561
13. Marx GH, Pethig R, Rousselet J (1997) The dielectrophoretic levitation of latex beads with reference to field-flow fractionation. *J Phys D Appl Phys* 30:2470–2477
14. Iliescu C, Xu GL, Samper V, Tay FEH (2005) Fabrication of a dielectrophoretic chip with 3D silicon electrodes. *J Micromech Microeng* 15:494–500
15. Park BY, Madou MJ (2005) 3-D electrode designs for flow-through dielectrophoresis systems. *Electrophoresis* 26:3745–3757
16. Wang L, Flanagan L, Jeon NL, Monuki E, Lee AP (2007) Dielectrophoresis switching with vertical sidewall electrodes for microfluidic flow cytometry. *Lab Chip* 7:1114–1120
17. Zhang YT, Bottausci F, Rao MP, Parker ER, Mezić I, MacDonald NC (2008) Titanium-based dielectrophoresis devices for microfluidic applications. *Biomed Microdevices* 10:509–517
18. Xia Y, Whitesides GM (1998) Soft lithography. *Annu Rev Mater Sci* 28:153–184
19. Niu X, Peng S, Liu L, Wen W, Sheng P (2007) Characterizing and patterning of PDMS-based conducting composites. *Adv Mater* 19:2682–2686
20. Cetin B, Kang Y, Wu Z, Li D (2009) Continuous particle separation by size via AC-dielectrophoresis using a lab-on-a-chip device with 3-D electrodes. *Electrophoresis* 30:766–772
21. Kang Y, Cetin B, Wu Z, Li D (2009) Continuous particle separation with localized AC-dielectrophoresis using embedded electrodes and an insulating hurdle. *Electrochim Acta* 54:1715–1720
22. Lewpiriyawong N, Yang C, Lam YC (2010) Continuous sorting and separation of microparticles by size using AC dielectrophoresis in a PDMS microfluidic device with 3-D conducting PDMS composite electrodes. *Electrophoresis* 31:2622–2631
23. Lewpiriyawong N, Kandaswamy K, Yang C, Ivanov V, Stocker R (2011) Microfluidic characterization and continuous separation of cells and particles using conducting poly (dimethyl siloxane) electrode induced alternating current-dielectrophoresis. *Anal Chem* 83:9579–9585
24. Lewpiriyawong N (2011) Continuous separation and manipulation of particles and cells using dielectrophoresis. Nanyang Technological University, Singapore
25. Jones TB (1995) *Electromechanics of particles*. Cambridge University Press, Cambridge
26. Morgan H, Green NG (2003) *AC electrokinetics: colloids and nanoparticles*. Research Studies, Philadelphia, PA
27. Suehiro J, Hamada R, Noutomi D, Shutou M, Hara M (2003) Selective detection of viable bacteria using dielectrophoretic impedance measurement method. *J Electrostat* 57:157–168
28. Wang L, Lu J, Marchenko SA, Monuki ES, Flanagan LA, Lee AP (2009) Dual frequency dielectrophoresis with interdigitated sidewall electrodes for microfluidic flow-through separation of beads and cells. *Electrophoresis* 30:782–791
29. Huang Y, Holzel R, Pethig R, Wang X-B (1992) Differences in the AC electrodynamic of viable and non-viable yeast cell determined through combined dielectrophoresis and electrorotation studies. *Phys Med Biol* 37(7):1499–1517
30. Marx GH, Huang Y, Zhou X-F, Pethig R (1994) Dielectrophoretic characterization and separation of micro-organisms. *Microbiology* 140:585–591
31. Lewpiriyawong N, Yang C, Lam YC (2012) Electrokinetically driven concentration of particles and cells by dielectrophoresis with DC-offset AC electric field. *Microfluid Nanofluid* 12:723–733
32. Church C, Zhu J, Wang G, Tzeng TJ, Xuan X (2009) Electrokinetic focusing and filtration of cells in a serpentine microchannel. *Biomicrofluidics* 3:044109
33. Wolfson A, Haddad N, Dlugy C, Tavor D, Shotland Y (2008) Baker's yeast catalyzed asymmetric reduction of methyl acetoacetate in glycerol containing systems. *Org Commun* 1(2):9–16
34. Tay FEH, Yu L, Panga AJ, Iliescu C (2007) Electrical and thermal characterization of a dielectrophoretic chip with 3D electrodes for cells manipulation. *Electrochim Acta* 52:2862–2868